Journal of Computational Chemistry

WILEY

Journal of COMPUTATIONAL CHEMISTRY

RESEARCH ARTICLE

Strength of FeS Bonds and Hydrogen Bonds in Small Molecule Inhibitors of Bacterioferritin: QM/MM and Local Mode Analysis

Marek Freindorf | Elfi Kraka

Chemistry Department, Southern Methodist University, Dallas, Texas, USA

Correspondence: Elfi Kraka (ekraka@smu.edu)

Received: 17 June 2025 | **Revised:** 12 October 2025 | **Accepted:** 18 October 2025

Funding: This work was supported by National Science Foundation (CHE 2102461).

Keywords: bacterioferritin | heme group | hydrogen bonds | local mode analysis | QM/MM

ABSTRACT

In this study, we computationally investigated the strength of FeS chemical bonds in heme groups and hydrogen bonds in bacterioferritin (BR) from *Pseudomonas aeruginosa* in the presence of small molecular inhibitors. The investigations were based on QM/MM calculations in both the ferric and ferrous oxidation states of BR, followed by Local Mode Analysis, with initial coordinates taken from available experimental x-ray structures of BR with ligands. Our results show that the FeS chemical bonds in both oxidation states were stronger, shorter, more covalent, and generally less polar than in the gas phase. In the ferrous state of the protein, the FeS bonds tended to be weaker, shorter, less covalent, and less polar than in the ferric state. On average, the hydrogen bonds in both oxidation states of the protein were stronger than a hydrogen bond in a water dimer, highlighting the influence of the protein environment on these interactions.

1 | Introduction

Many enzymatic reactions across diverse metabolic processes involve the transition metal iron (Fe) [1]. In bacteria Fe can exist mainly in two oxidation states, as water insoluble ferric (Fe^{3+}) and soluble ferrous (Fe^{2+}) ions. The bacterial Fe homeostasis requires a right balance between these two oxidation states of Fe, because an excess of the low solubility ferric Fe leads to a reduced Fe bioavailability, while an excess of the soluble ferrous Fe can react with O_2 and H_2O_2 generating reactive oxygen species such as superoxide or hydroxyl radicals. Therefore, a correct concentration ratio between ferric and ferrous Fe, is important for storage and utilization of Fe and for preventing iron–induced toxicity [2]. Fe is accumulated in bacteria in the form of a ferric Fe mineral, using a protein bacterioferritin (BF) which is a key protein for bacteria homeostasis. The correct ferric to ferrous ratio is regulated in bacteria by an associated ferredoxin protein (FD), which binds to the surface of BF by a protein–protein interaction [3]. Small molecules can also bind to the surface of BF and inhibit the protein–protein interaction with FD, which can unbalance the bacterial Fe homeostasis leading to a cell death [4]. BF is composed of 24 protein subunits that assemble into a spherical hollow structure with an external diameter of about 120 Å and an internal diameter of about 80 Å [3–5]. There are generally three types of Fe sites within BF: a dinuclear Fe site, a b–type heme group, and a single Fe ion site. The protein chains of BF are connected by 12 heme groups through the side chains of two methionine residues. The overall structure of BF also depends on the Fe oxidation state, as confirmed by experimental x–ray studies of BF from *Azotobacter vinelandii* [6]. The transition between the ferric and ferrous oxidation states is responsible for Fe mineralization in BF. Numerous experimental studies have highlighted the importance of the heme groups in BF activity, including their role in Fe release from the BF biomineral

[3, 4, 7–21]. The heme groups of BF facilitate electron transfer between the dinuclear Fe site and the ferric mineral core, leading to the formation of soluble ferrous Fe ions.

In this study, we computationally investigated a strength of FeS chemical bonds in the heme groups in both the ferric and the ferrous oxidation state, involving the small molecular inhibitors in the binding sites of BR from *Pseudomonas aeruginosa*, which experimental x–ray structures have been reported [4]. We have also analyzed a strength of hydrogen bonds between the molecular ligands and the BR binding sites in both Fe oxidation states. The objective of this study, was to find any relation between the strength of the FeS chemical bonds in the different Fe oxidation states, and the strength of the hydrogen bonds formed between the ligands and the BR binding site. We also correlated in this study the strength of the FeS bonds, with other bond properties such as a bond length, a bond covalent character, and a bond polarity. For the hydrogen bonds we correlated their strength with a hydrogen bond length.

2 | Methodology

The main objective of this study was to calculate precisely the strength of chemical and hydrogen bonds in the protein active sites. Such calculations require advanced methods capable of accurately describing the electronic structure of the active site and its interactions with the surrounding protein. For this reason, we employed a combined QM/MM approach, which enables reliable treatment of active sites together with the overall protein geometry [22, 23]. The starting coordinates for the QM/MM calculations were taken from x-ray structures of BF with small molecular inhibitors from *Pseudomonas aeruginosa* (PDB entries: 6NLG for ligand **L1**, 6NLI for **L2**, 6NLK for **L3**, 6NLL for **L4**, 6NLM for **L5** and 6NLN for **L6**; see Figure 1) [4]. From each structure we selected two protein chains connected by the heme group and the ligand in the binding site. Because the experimental geometries lack hydrogen atoms, they were added following AMBER protonation rules [24]. To mimic the aqueous environment, each system was embedded in a TIP3P [25] water sphere of 16 Å radius centered at the heme Fe atom. Sodium counter–ions were added for charge neutrality, and the systems were minimized at the MM level with AMBER. The QM region comprised the heme group, the side chains of two methionines bound to it (Figure 2a), and the ligand. Bonds connecting the heme and methionines to the protein backbone were cut and saturated with link hydrogen atoms. The remainder of the protein and water molecules formed the MM region. Calculations were performed for the ferric (doublet) and ferrous (singlet) states using ONIOM [26] at the PBE0/6-31G(d,p)/AMBER level [27, 28]. Geometry optimizations were followed by vibrational frequency analyses.

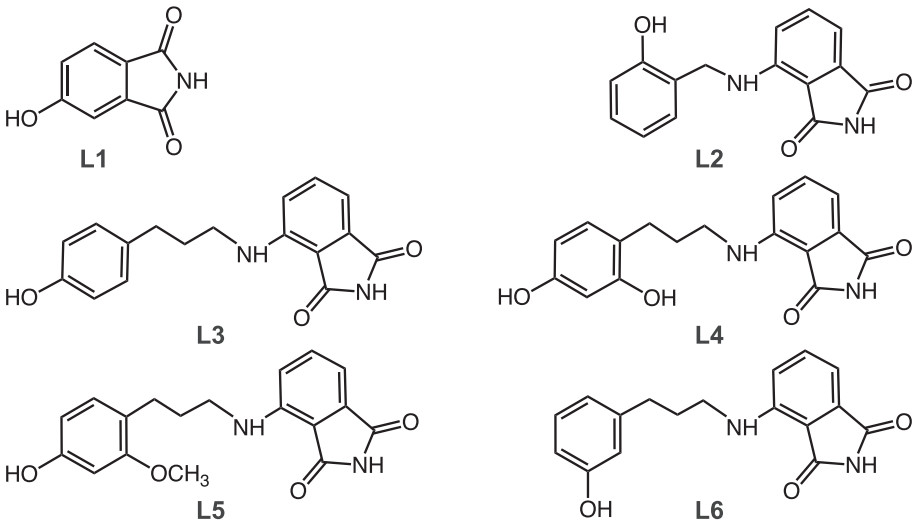

FIGURE 1 | Sketches of molecular ligands of bacterioferritin investigated in this study.

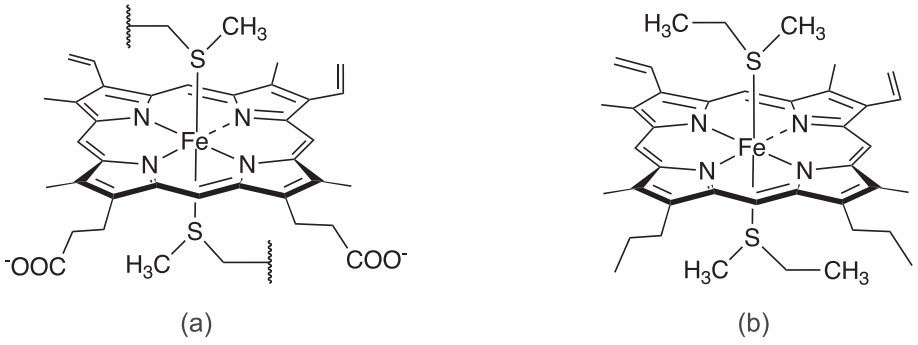

FIGURE 2 | Sketches of heme QM models investigated in this study; (a) QM/MM calculations; (b) gas phase calculations.

No imaginary frequencies were found, confirming local minima. The PBE0 functional, well suited for transition metal complexes [27, 29–31], had also been used successfully in our earlier QM/MM studies of hemoproteins [32, 33]. As validation, the FeN bond length of a bishistidyl heme model (1.965 Å) agreed with the x-ray value of bis(1-methylimidazole) (meso-tetramesitylporphinato) ferric Fe (1.970 Å) [34]. To assess protein effects, we also carried out gas-phase calculations on a simplified heme model (Figure 2b) and on a water dimer. Bond strengths of the FeS bonds and hydrogen bonds were then determined using Local Mode Analysis (LMA) [35]. Originally developed by Konkoli and Cremer [36–40], LMA has been extensively applied to quantify covalent bonds [41–54], non–covalent interactions [52, 55–69], and hydrogen bonds [70–80], and has been used by us in previous QM/MM studies of hemoproteins [32, 33]. To compare bond strengths with standard single and multiple bond concepts, local mode force constants (k^a) were converted into relative bond strength orders (BSO) via the relation $BSO = A \times (k^a)^B$, following the generalized Badger rule [41, 49]. Parameters A and B were obtained from reference molecules using Mayer bond orders [81–83]. For transition metal bonds, $CuCH_3$ ($k^a = 3.243$ mDyn/Å, BSO = 1.005) and $NiCH_2$ ($k^a = 5.568$ mDyn/Å, BSO = 1.894) gave $A = 0.2530$, $B = 1.1724$. For hydrogen bonds, F_2H^- ($k^a = 1.340$ mDyn/Å, BSO = 0.5) and HF ($k^a = 9.804$ mDyn/Å, BSO = 1.0) yielded $A = 0.4515$, $B = 0.3483$. Covalent character was further assessed within Bader's QTAIM framework [84–86] using the Cremer–Kraka criterion: [87–89] a negative energy density at the bond critical point indicates covalency, while a positive value indicates electrostatics. All DFT calculations were performed with Gaussian [90], LMA with LModeA [91], charges with NBO [92], and QTAIM with AIMALL [93]. Chemical sketches of the ligands in their binding sites are shown in Figures 3 and 4. In addition, Figure S1 shows the relationships between the SFeS bond angle and the force constants for both ferric and ferrous states, as well as the correlations between the FeS and SFeS force constants. Figures S2–S5 present the optimized geometries of the active sites and protein–ligand complexes. The coordinates of the optimized geometries of the ligands in the binding sites investigated in this study are also provided in the Supporting Information.

3 | Results and Discussion

3.1 | FeS Chemical Bonds of Heme Groups

Results of the FeS bond properties such as the bond length R, the local mode force constant k^a, the local mode frequency ω^a, the energy density at a bond critical point H_ρ, the Fe and S atomic charge difference ΔQ, and the bond strength order BSO, in the heme group of BR with different ligands are presented in Table 1 for the ferric state and in Table 2 for the ferrous state. The label **L1oFeSa** denotes the properties of the FeS bond for the protein with the ligand **L1** in the oxidized (ferric) state of the bond in the distal heme pocket, while the label **L1oFeSb** refers to the proximal heme pocket. The label **L1rFeSa** is related to the properties of this bond in the reduced (ferrous) protein state. Similarly for the proteins with the other five ligands (**L2**, **L3**, **L4**, **L5**, and **L6**), while **GoFeSa** and **GoFeSb** are the FeS bond properties in the oxidized state of the gas phase model. Figure 5a–d show graphical representations of the relations between BSO and k^a, as well between R and k^a, while Figure 6a–d the relations between H_ρ and k^a, in addition between ΔQ and k^a, in the ferric and ferrous states. According to Figure 5a, the strength of the FeS bond in the ferric state of the proteins (the average $k^a = 0.855$ mDyn/Å) is generally bigger that in the gas phase model (the average $k^a = 0.621$ mDyn/Å), with the outliner for the FeS bond strength in the ligand **L6** (the average $k^a = 0.486$ mDyn/Å).

Similarly, according to Figure 5b, the strength of the FeS bond in the ferrous state (the average $k^a = 0.719$ mDyn/Å) is bigger than in the gas phase (the average $k^a = 0.544$ mDyn/Å), which generally indicates that the protein environment increases the FeS bond strength in both oxidation states of the proteins. Moreover, we observed in our study that the FeS bond in the ferrous state, is weaker then in the ferric state in both environments such as the protein ($k^a = 0.855$ and 0.719 mDyn/Å, in the ferric and ferrous state, respectively) and the gas phase ($k^a = 0.621$ and 0.544 mDyn/Å). The only exception is the protein with the ligand **L6**, for which this change of the oxidation state makes the FeS bond stronger in the protein ($k^a = 0.486$ and 0.744 mDyn/Å, in the ferric and ferrous state, respectively). Although a shorter chemical bond is generally expected to have a bigger strength, there is a number of papers showing an opposite effect [42, 48, 50, 52, 94–96]. Therefore, it is interesting to verify the relation between the FeS bond length and its local mode force constant in the investigated protein systems. According to Figure 5c there is a relatively good correlation ($R^2 = 0.9156$) between the FeS bond length R and its local mode force constant k^a in the ferric state, with two outliners namely the protein with the ligand **L6** and the gas phase. Similarly, according to Figure 5d, there is also a good correlation ($R^2 = 0.9067$) between the FeS bond length R and its local mode force constant k^a in the ferrous state, showing that in both oxidation states a stronger FeS bond correlates with a smaller bond length. The change of the oxidation state from ferric to ferrous generally makes the bond length R smaller (the average bond length R = 2.359 and 2.341 Å, in the ferric and ferrous state, respectively). Similarly in the gas phase, the change of the oxidation state makes the FeS bond shorter (R = 2.384 and 2.366 Å). However, in both oxidation states the average bond length R in the protein (R = 2.359 and 2.341 Å) is smaller than in the gas phase (R = 2.384 and 2.366 Å), which shows how the protein environment changes the geometry of the heme group.

Figure 6a,b present the relation between the energy density at a bond critical point H_ρ and the local mode force constant k^a for the ferric and ferrous states. According to Figure 6a, there is a relatively good correlation ($R^2 = 0.9739$) between these two quantities in the ferric state, with the two outliners namely the protein with the ligand **L6** and the gas phase, indicating that a stronger FeS bond corresponds to a more negative energy density and a more covalent bond character. The FeS bond in the ferric state of the protein has a more covalent character than in the gas phase (the average $H_\rho = -0.0196$ and -0.0174 Hartree/Bohr^3, respectively). Similarly, according to Figure 6b, in the ferrous state there is a good correlation ($R^2 = 0.9399$) between the energy density at a bond critical point H_ρ and the local mode force constant k^a, where the FeS bond in the protein has a more covalent character than in the gas

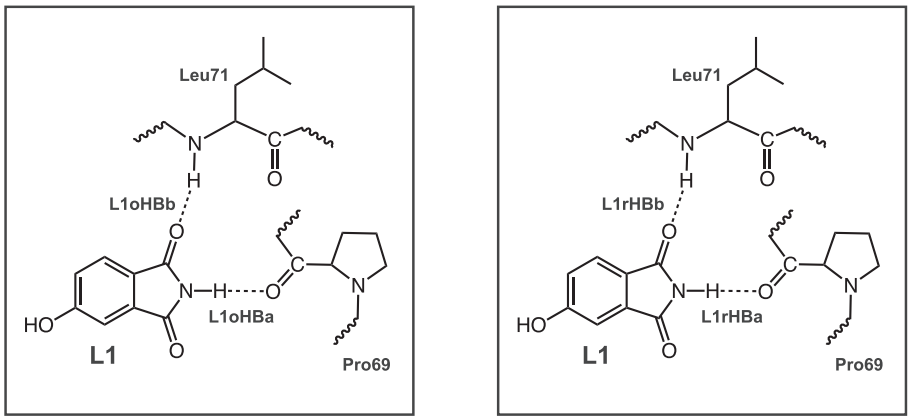

(a)

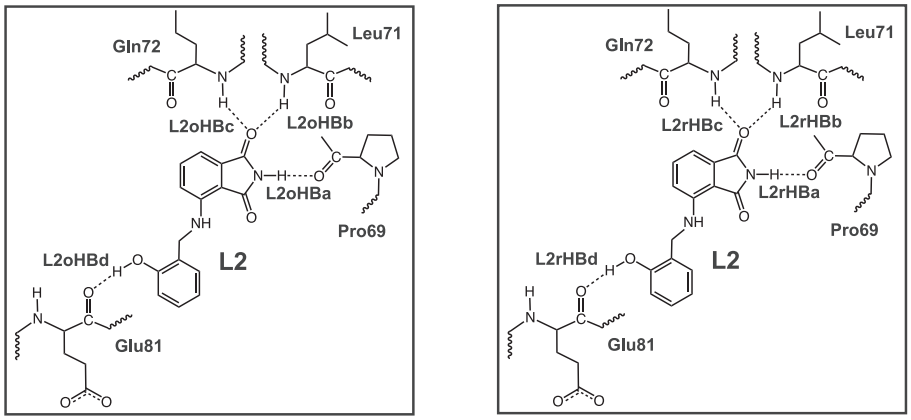

(b)

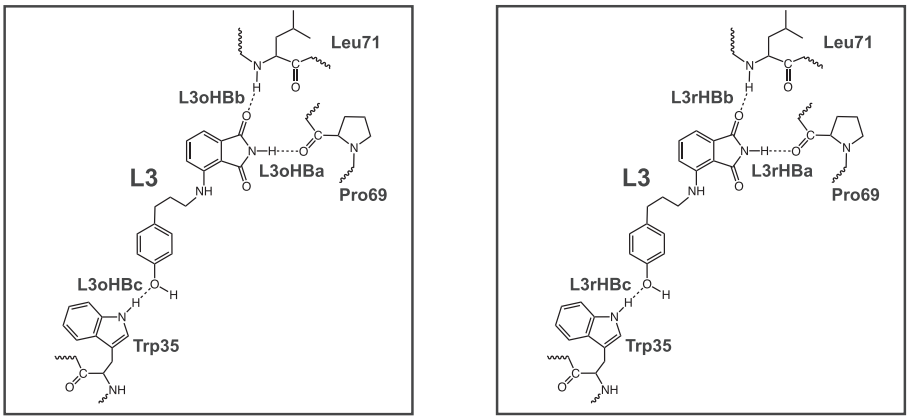

(c)

FIGURE 3 | Sketches of hydrogen bonds for ligands in bacterioferritin, (left) oxidized, (right) reduced; (a) L1; (b) L2; (c) L3.

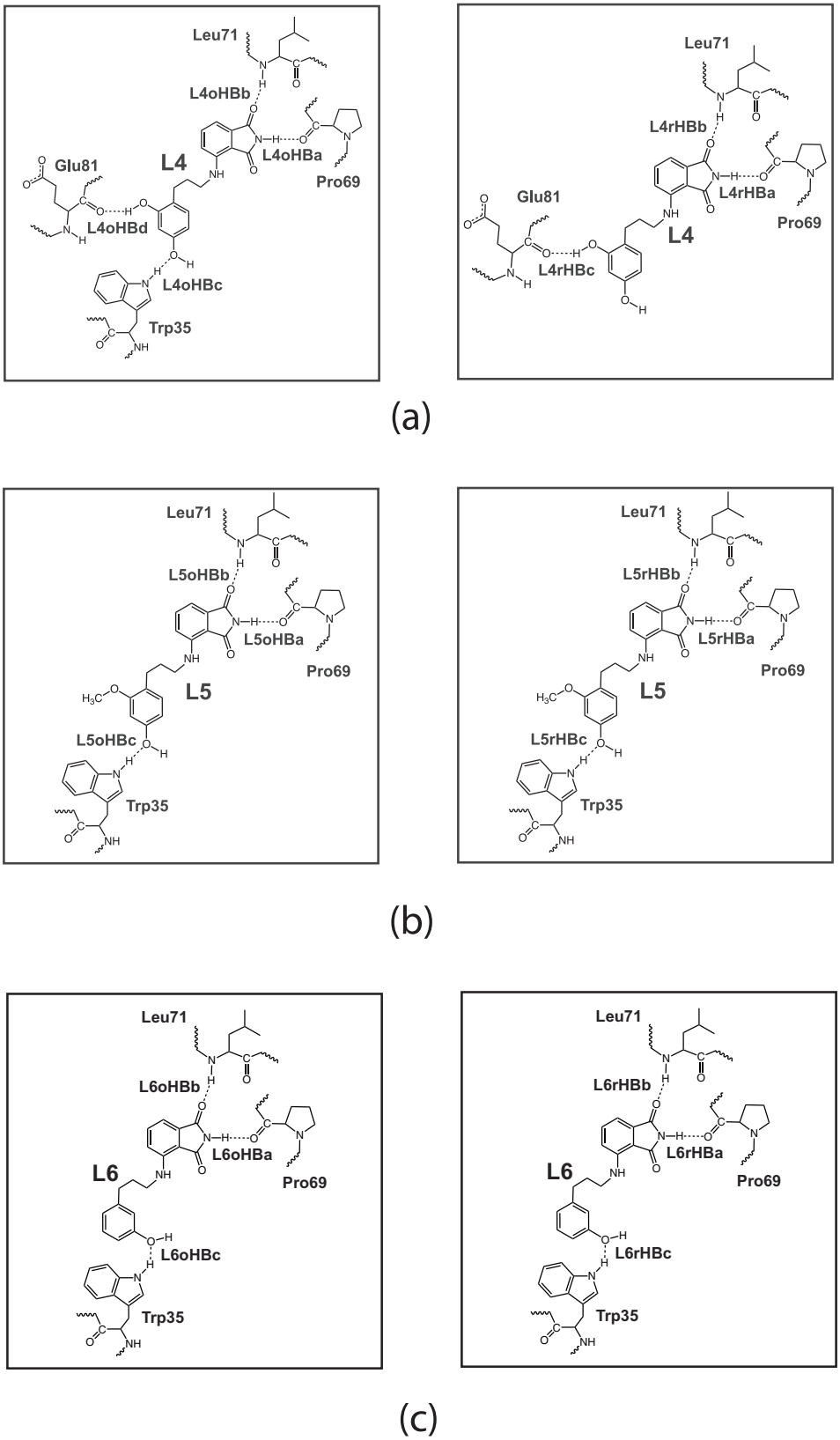

FIGURE 4 | Sketches of hydrogen bonds for ligands in bacterioferritin, (left) oxidized, (right) reduced; (a) L4; (b) L5; (c) L6.

phase (the average $H_\rho = -0.0129$ and -0.0106 Hartree/Bohr^3, respectively). The change of the oxidation state from ferric to ferrous in the protein, makes the FeS bond less covalent ($H_\rho = -0.0196$ and -0.0129 Hartree/Bohr^3, respectively), and similarly in the gas phase ($H_\rho = -0.0174$ and -0.0106 Hartree/Bohr^3). The charge difference ΔQ between the Fe and S atoms in the FeS bonds is correlated with the local mode force constant k^a for the ferric and ferrous states in Figure 6c,d.

TABLE 1 | Bond length R, local mode force constant k^a, local mode frequency ω^a, energy density at a bond critical point H_ρ, Fe and S atomic charge difference ΔQ, and bond strength order BSO of FeS chemical bond, in ferric state of bacterioferritin with molecular ligands investigated in this study.

	R	k^a	ω^a	H_ρ	ΔQ	
Bond	**Å**	**mDyn/Å**	**cm^{-1}**	**Hartree/$Bohr^3$**	**e**	**BSO**
L1oFeSa	2.400	0.750	250	−0.0175	0.579	0.181
L1oFeSb	2.399	0.748	250	−0.0172	0.585	0.180
L2oFeSa	2.341	0.892	273	−0.0201	0.542	0.221
L2oFeSb	2.345	0.857	267	−0.0199	0.537	0.211
L3oFeSa	2.337	0.906	275	−0.0208	0.533	0.225
L3oFeSb	2.342	0.874	270	−0.0200	0.538	0.216
L4oFeSa	2.375	0.855	267	−0.0192	0.565	0.211
L4oFeSb	2.385	0.786	256	−0.0182	0.567	0.191
L5oFeSa	2.323	0.981	286	−0.0225	0.524	0.247
L5oFeSb	2.338	0.905	275	−0.0202	0.530	0.225
L6oFeSa	2.367	0.483	201	−0.0175	0.554	0.108
L6oFeSb	2.363	0.489	202	−0.0177	0.552	0.109
GoFeSa	2.381	0.632	230	−0.0176	0.562	0.148
GoFeSb	2.386	0.609	225	−0.0173	0.566	0.141

Note: For labels see the text.

TABLE 2 | Bond length R, local mode force constant k^a, local mode frequency ω^a, energy density at a bond critical point H_ρ, Fe and S atomic charge difference ΔQ, and bond strength order BSO of FeS chemical bond, in ferrous state of bacterioferritin with molecular ligands investigated in this study.

	R	k^a	ω^a	H_ρ	ΔQ	
Bond	**Å**	**mDyn/Å**	**cm^{-1}**	**Hartree/$Bohr^3$**	**e**	**BSO**
L1rFeSa	2.369	0.593	222	−0.0114	0.421	0.137
L1rFeSb	2.382	0.546	213	−0.0104	0.430	0.124
L2rFeSa	2.340	0.731	247	−0.0127	0.396	0.175
L2rFeSb	2.334	0.735	248	−0.0137	0.385	0.176
L3rFeSa	2.345	0.718	245	−0.0127	0.394	0.172
L3rFeSb	2.322	0.785	256	−0.0140	0.381	0.191
L4rFeSa	2.333	0.759	252	−0.0130	0.381	0.183
L4rFeSb	2.318	0.802	259	−0.0140	0.384	0.195
L5rFeSa	2.338	0.729	247	−0.0136	0.394	0.175
L5rFeSb	2.335	0.743	249	−0.0129	0.399	0.179
L6rFeSa	2.352	0.689	240	−0.0123	0.394	0.163
L6rFeSb	2.320	0.799	258	−0.0144	0.388	0.194
GrFeSa	2.364	0.548	214	−0.0107	0.397	0.125
GrFeSb	2.367	0.539	212	−0.0105	0.400	0.123

Note: For labels see the text.

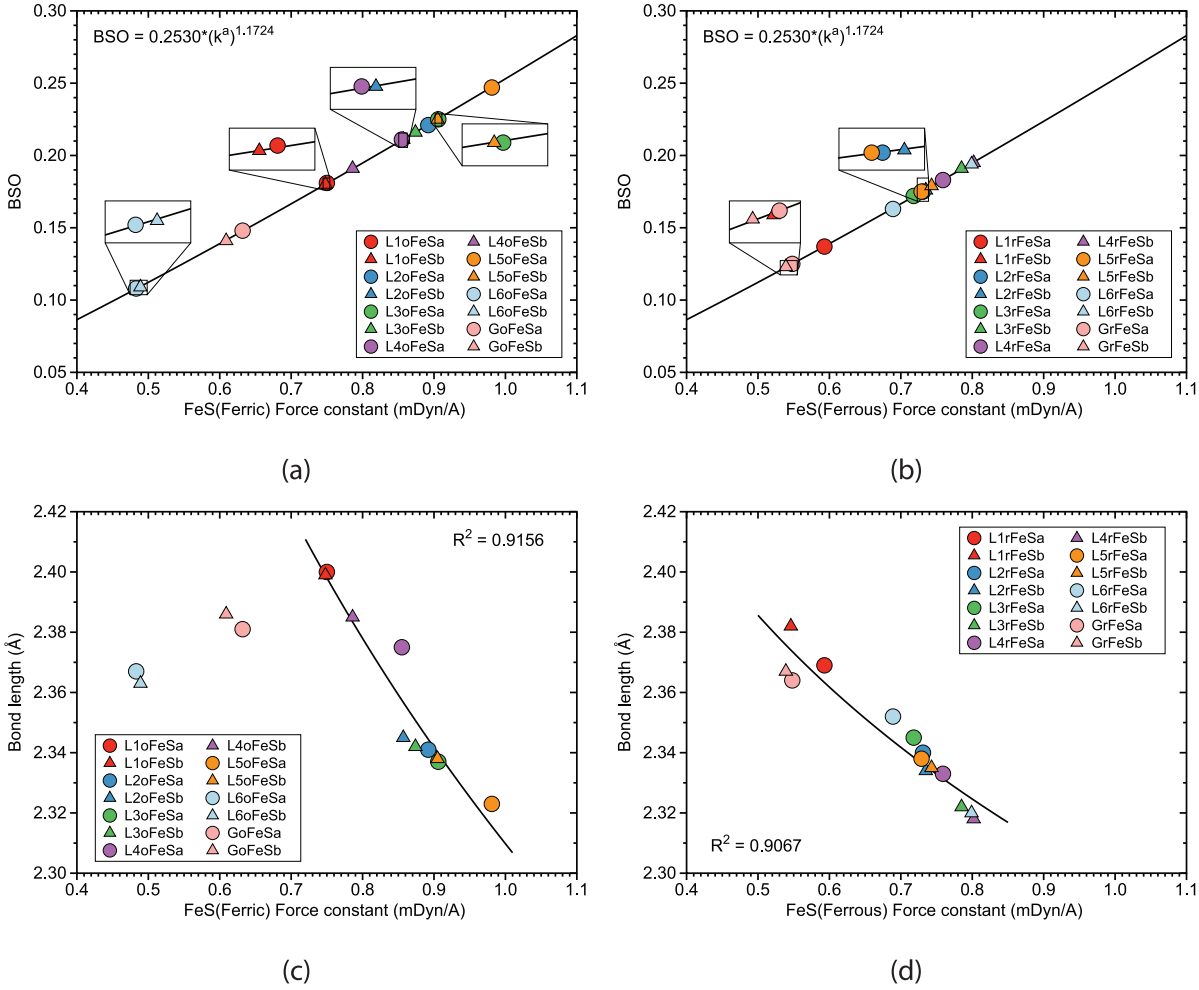

FIGURE 5 | Properties of FeS chemical bonds in bacterioferritin and gas phase models. (a) Functional relationship between local mode force constant k^a and BSO for ferric state. (b) Functional relationship between local mode force constant k^a and BSO for ferrous state. (c) Relation between local mode force constant k^a and bond length R for ferric state. (d) Relation between local mode force constant k^a and bond length R for ferrous state. For molecular labels, see the text.

According to Figure 6c, there is a relatively small correlation ($R^2 = 0.8639$) between these quantities in the ferric state, with the two outliners the protein with the ligand **L6** and the gas phase, showing that a stronger FeS bonds correlates with a smaller charge difference. Generally, the average charge difference in the ferric state of the protein is smaller than in the gas phase ($\Delta Q = 0.550$ and 0.564 e, respectively). Similarly, in the ferrous state the correlation between ΔQ and k^a is even smaller ($R^2 = 0.5602$), and the average charge difference in this oxidation state of the protein is similar to in the gas phase ($\Delta Q = 0.397$ and 0.399 e). Changing the oxidation state from ferric to ferrous in the protein, makes the charge difference smaller ($\Delta Q = 0.550$ and 0.397 e), and similarly in the gas phase ($\Delta Q = 0.564$ and 0.399 e).

Generally, we observe in our calculations that the FeS chemical bond in the ferric state of the protein is stronger, shorter, more covalent, and less polar than in the gas phase, however there are two outliners namely the protein with the ligand **L6** and the gas phase model. Similarly, the FeS bond in the ferrous state of the protein is stronger, shorter, more covalent, and similarly polar than in the gas phase, without outliners. In the protein ferrous state the FeS bonds are weaker, shorter, less covalent, and less polar than in the ferric state. The similar changes of the FeS bond properties are observed in our calculations in the gas phase.

3.2 | Hydrogen Bonds Between Ligands And Proteins

The properties of the hydrogen bonds between the ligands and the surrounding amino acids of the protein binding sites for the ferric oxidation state are presented in Table 3, and for the ferrous state in Table 4. The protein environment can change the hydrogen bonding interactions between the investigated ligands and the side chains of amino acids in the binding pocket. In order to analyze this effect, we have also calculated in the gas phase (without the protein surrounding) a simple water dimer forming a hydrogen bond between water monomers (**H2O-HOH**), and the results of this calculations are also presented in Tables 3 and 4 as a hydrogen bond strength reference. In order to calculate the energy density at a bond critical point and the atomic charge difference for hydrogen bonded

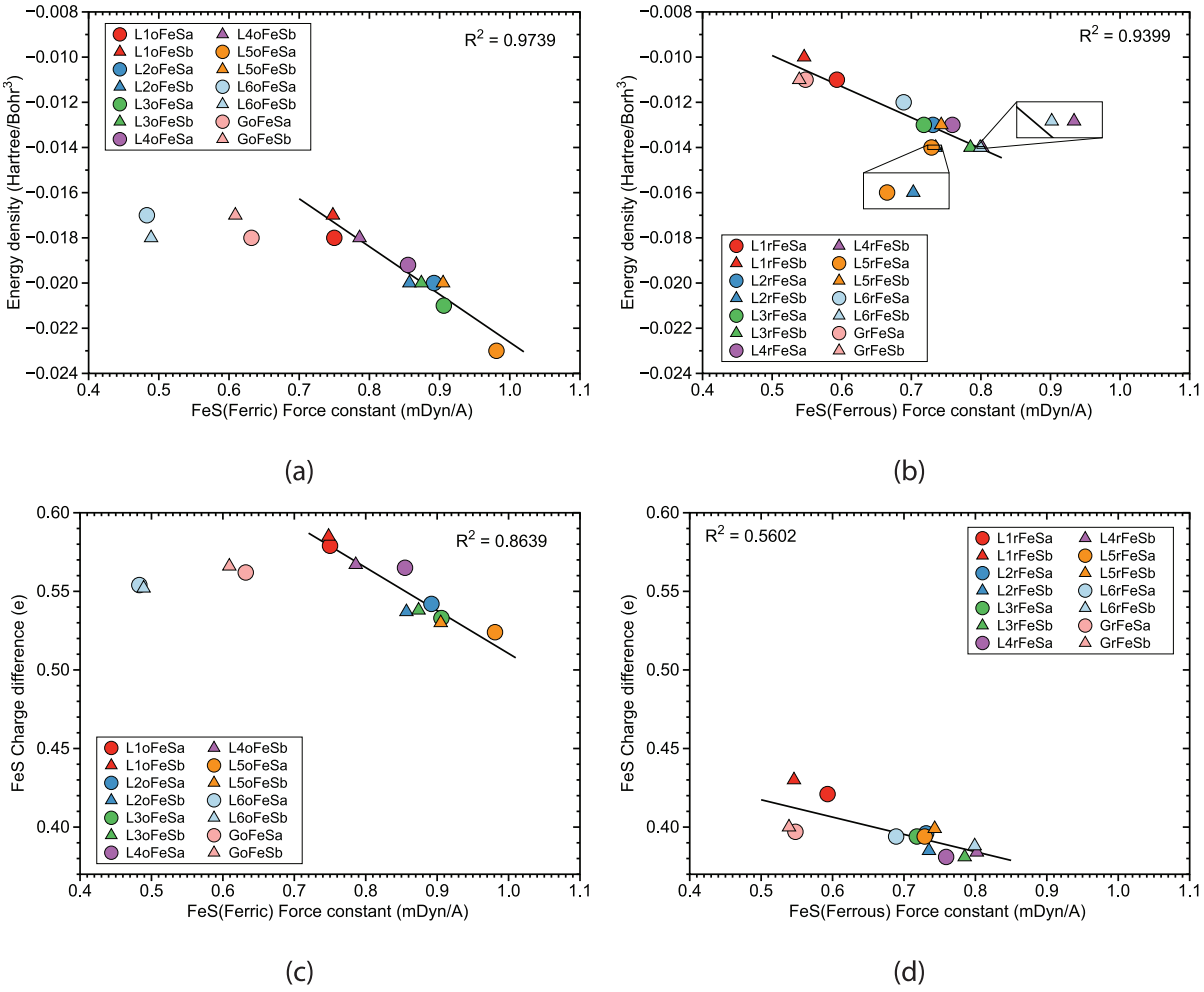

FIGURE 6 | Properties of FeS chemical bonds in bacterioferritin and gas phase models. (a) Relation between local mode force constant k^a and energy density for ferric state. (b) Relation between local mode force constant k^a and energy density for ferrous state. (c) Relation between local mode force constant k^a and charge difference for ferric state. (d) Relation between local mode force constant k^a and charge difference for ferrous state. For molecular labels, see the text.

complexes, both monomers of a dimer should be present in the QM part of the QM/MM calculations. Because in our study only the ligand is included in the QM part, we present here only results of the bond length R, the local mode force constant k^a, the local mode frequency ω^a, and the bond strength order BSO for the hydrogen bonds between the ligands and the protein. Including all amino acids forming hydrogen bonds with the ligands in the QM part, would require much longer and more advanced QM/MM computations, which is beyond the scope of this manuscript. Moreover, hydrogen bonds between QM and MM atoms are pretty well defined in the standard QM/MM calculations [97]. The labels of the hydrogen bonds are formed in the similar way as the labels of the FeS chemical bonds investigated in this study, where the characters "a", "b", and so on, indicate different positions of the hydrogen bonds, which chemical sketches are presented in Figures 3 and 4 and also in Figures S2–S5. The relations between the hydrogen bond properties are presented in Figure 7a–d. According to Figures 3, 4, and S2–S5, the number and the form of the hydrogen bonds between the ligand and the protein depends on a particular ligand and the oxidation state of the protein.

The ligand **L1** (5–hydroxyisoindoline–1,3–dione) is the simplest ligand in our calculations, forming two hydrogen bonds with the protein in the ferric states, namely **L1oHBa** (red circle in Figure 7) and **L1oHBb** (red triangle in Figure 7). The **L1oHBa** hydrogen bond is of a N–H ⋯ O type, where the hydrogen atom donor is from the ligand, while the oxygen atom is from Pro69 of the protein. **L1oHBb** is also the N–H ⋯ O type, but the hydrogen atom donor is from Leu71 of the protein and the oxygen atom is from the ligand. According to Figure 7a **L1oHBa** and **L1oHBb** are relatively weak in the ferric states of the protein ($k^a = 0.141$ and 0.210 mDyn/Å, respectively), and their strengths are smaller than the hydrogen bond strength in the water dimer ($k^a = 0.214$ mDyn/Å, pink circle in Figure 7). Similarly, according to Figure 7b, **L1rHBa** and **L1rHBb** in the ferrous state are also weak.

The ligand **L2** is a modification of **L1** and it involves the o–hydroxyphenyl ring capable of an additional hydrogen bond formation. There are four hydrogen bonds of **L2** in the ferric state, namely **L2oHBa**, **L2oHBb**, **L2oHBc**, and **L2oHBd**. **L2oHBa** (blue circle in Figure 7) has the same N–H ⋯ O character as in the ligand **L1**, but contrary to **L1** it is relatively strong ($k^a = 0.602$

TABLE 3 | Bond length R, local mode force constant k^a, local mode frequency ω^a, and bond strength order BSO of hydrogen bonds between ligands and bacterioferritin, in ferric state.

	R	k^a	ω^a	
Bond	**Å**	**mDyn/Å**	**cm^{-1}**	**BSO**
L1oHBa	1.932	0.141	503	0.228
L1oHBb	1.936	0.210	614	0.262
L2oHBa	1.763	0.602	1038	0.378
L2oHBb	2.249	0.036	252	0.142
L2oHBc	2.155	0.055	313	0.164
L2oHBd	1.801	0.388	834	0.325
L3oHBa	1.807	0.411	858	0.331
L3oHBb	1.885	0.269	694	0.286
L3oHBc	2.238	0.053	308	0.162
L4oHBa	1.753	0.664	1090	0.392
L4oHBb	1.885	0.281	709	0.290
L4oHBc	1.829	0.320	757	0.304
L4oHBd	2.231	0.055	315	0.164
L5oHBa	1.754	0.647	1077	0.388
L5oHBb	1.915	0.213	617	0.263
L5oHBc	2.035	0.106	436	0.207
L6oHBa	1.740	0.685	1108	0.396
L6oHBb	1.960	0.159	534	0.238
L6oHBc	2.130	0.061	331	0.170
H_2O-HOH	1.906	0.214	619	0.264

Note: For labels see the text.

TABLE 4 | Local mode bond length R, local mode force constant k^a, local mode frequency ω^a, and bond strength order BSO of hydrogen bonds between ligands and bacterioferritin, in ferrous state.

	R	k^a	ω^a	
Bond	**Å**	**mDyn/Å**	**cm^{-1}**	**BSO**
L1rHBa	1.907	0.162	538	0.240
L1rHBb	1.943	0.200	599	0.258
L2rHBa	1.774	0.546	989	0.366
L2rHBb	2.216	0.032	239	0.136
L2rHBc	2.184	0.044	282	0.152
L2rHBd	1.794	0.400	847	0.328
L3rHBa	1.813	0.396	842	0.327
L3rHBb	1.915	0.217	623	0.265
L3rHBc	2.280	0.042	274	0.150
L4rHBa	1.830	0.367	811	0.318
L4rHBb	1.841	0.365	808	0.318
L4rHBc	1.804	0.367	810	0.318
L5rHBa	1.751	0.644	1074	0.387
L5rHBb	1.906	0.244	661	0.276
L5rHBc	2.846	0.005	90	0.071
L6rHBa	1.782	0.524	969	0.361
L6rHBb	1.951	0.188	581	0.252
L6rHBc	2.531	0.011	143	0.094
H2O-HOH	1.906	0.214	619	0.264

Note: For labels see the text.

mDyn/Å). **L2oHBb** and **L2oHBc** (blue triangle and square in Figure 7) are two components of the bifurcated hydrogen bond of the N–H ⋯ O type, where Leu71 and Gln72 of the protein are the hydrogen atom donors, while the oxygen atom is from the ligand, and both components are relatively weak (k^a = 0.036 and 0.055 mDyn/Å, respectively). **L2oHBd** (blue romb in Figure 7) is a hydrogen bond of the O–H ⋯ O type, formed between the hydroxy group of the ligand as a hydrogen atom donor, and the oxygen atom of Glu81. **L2oHBd** is relatively strong (k^a = 0.388 mDyn/Å), however is weaker than the strongest hydrogen bond of this ligand **L2oHBa** (k^a = 0.602 mDyn/Å). In the ferrous state of the protein with **L2** (blue marks in Figure 7b), the strength of the hydrogen bonds is similar as in the ferric state, however the strongest hydrogen bond in this group **L2rHBa** is slightly weaker than in the ferric state **L2oHBa** (k^a = 0.546 and 0.602 mDyn/Å, respectively).

The ligand **L3** has the hydroxyphenyl ring similarly as **L2**, however the hydroxy group is in the *para* position, and the hydroxyphenyl ring is attached to the main part of the ligand (the isoindoline–1,3–dione group) by a longer hydrocarbon chain, increasing flexibility of the entire molecule. There are three hydrogen bonds formed by **L3** in the ferric state, such as **L3oHBa**, **L3oHBb**, and **L3oHBc**. **L3oHBa** has the similar hydrogen bond character as **L1oHBa** and **L2oHBa**, and it is the strongest one in **L3** (green circle, k^a = 0.411 mDyn/Å). **L3oHBc** is the weakest one (green square, k^a = 0.053 mDyn/Å), it has the N–H ⋯ O character, and is formed between Trp35 acting as a hydrogen atom donor, and the oxygen atom of the ligand. **L3** in the ferrous state, forms similar hydrogen bonds with similar strengths (**L3rHBa** green circle, **L3rHBb** green triangle, and **L3rHBc** green square in Figure 7b, k^a = 0.396, 0.217, and 0.042 mDyn/Å, respectively).

The next ligand investigated in our study **L4**, has two hydroxy groups in the phenyl ring (*ortho* and *para*), and a similar longer hydrocarbon chain linking the phenyl ring with the isoindoline group. In the ferric state **L4** forms four hydrogen bonds with the protein, such as **L4oHBa**, **L4oHBb**, **L4oHBc**, and **L4oHBd** (purple marks in Figure 7a). **L4oHBa** (purple circle), **L4oHBb** (purple triangle), and **L4oHBc** (purple square) have the similar hydrogen bond characters as **L3**, however with bigger strengths (k^a = 0.664, 0.281, and 0.320 mDyn/Å, respectively). **L4oHBd** is a weak hydrogen bond (purple rhomb, k^a = 0.055 mDyn/Å) of the O–H ⋯ O character, formed between the hydroxy group of the ligand acting

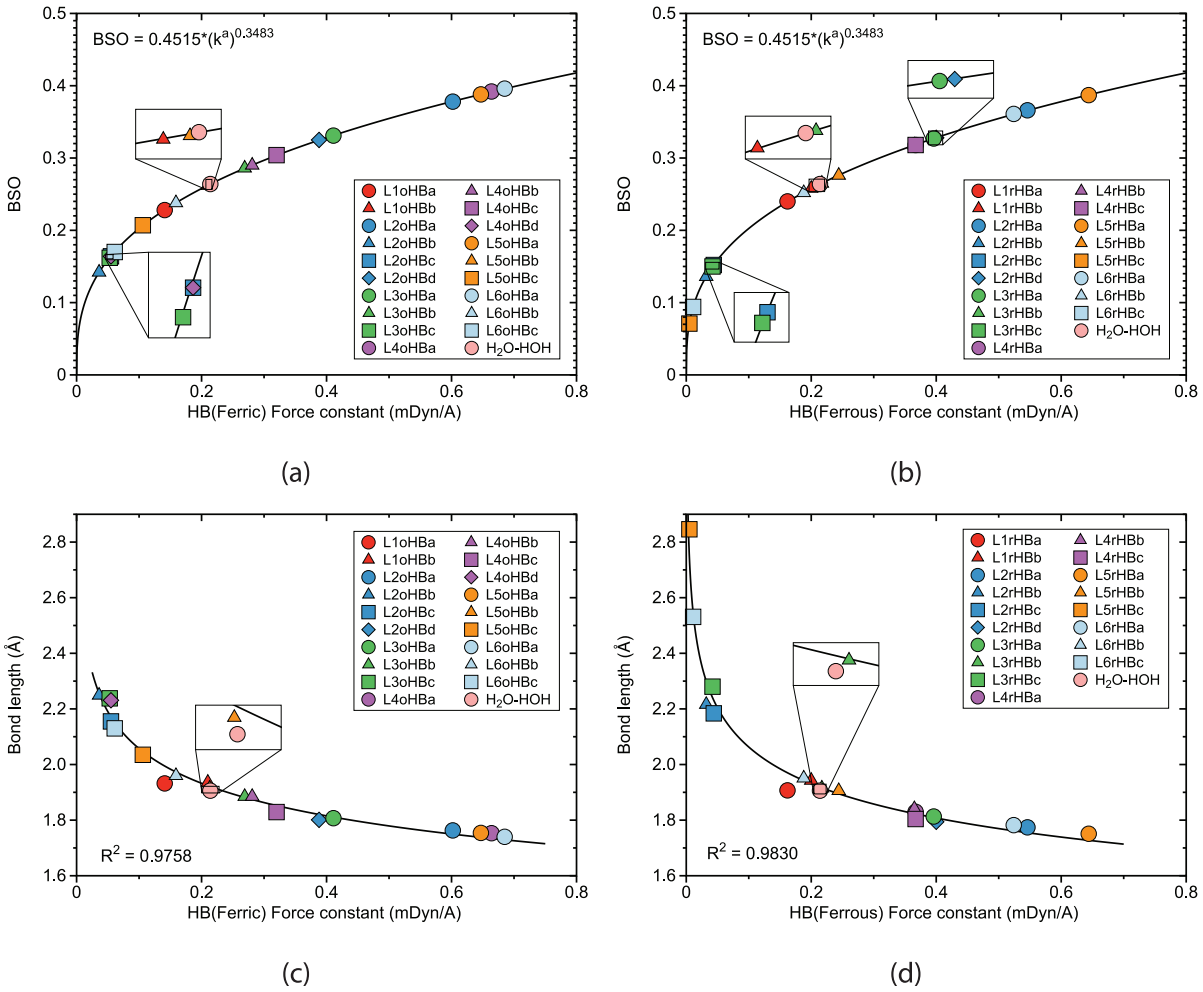

FIGURE 7 | Properties of hydrogen bonds between ligands and bacterioferritin. (a) Functional relationship between local mode force constant k^a and BSO for ferric state. (b) Functional relationship between local mode force constant k^a and BSO for ferrous state. (c) Relation between local mode force constant k^a and bond length R for ferric state. (d) Relation between local mode force constant k^a and bond length R for ferrous state. For molecular labels, see the text.

as a hydrogen atom donor, and the oxygen atom of Glu81. In the ferrous state **L4** forms only three hydrogen bonds, namely **L4rHBa**, **L4rHBb**, and **L4rHBc** (purple marks in Figure 7b), and the hydrogen bond with Trp35 has not been found in our calculations. **L4rHBa** and **L4rHBb** have the similar hydrogen bond character as in the ferric state, while **L4rHBc** which is a hydrogen bond between the ligand and Glu81, corresponds to **L4oHBd** in the ferric state. It is interesting to note that in the ferrous state, all three hydrogen bonds **L4rHBa**, **L4rHBb**, and **L4rHBc** have similar strengths (k^a = 0.367, 0.365, and 0.367 mDyn/Å, respectively).

The ligand **L5** is a modification, which has the methoxy instead of the hydroxy group in the *ortho* position of the phenyl ring. This modification prevents formation of a hydrogen bond with Glu81, therefore in **L5** there are only three hydrogen bonds in the ferric state (orange marks in Figure 7a), such as **L5oHBa** (circle), **L5oHBb** (triangle), and **L5oHBc** (square), which characters are the same as in **L4**, and they have similar strengths as in **L4** (k^a = 0.647, 0.213, and 0.106 mDyn/Å, respectively). In the ferrous state **L5** forms three hydrogen bonds (orange marks in Figure 7b), namely **L5rHBa** (orange circle, k^a = 0.644 mDyn/Å), **L5rHBb** (orange triangle, k^a = 0.244 mDyn/Å) and **L5rHBc** (orange square, k^a = 0.005 mDyn/Å). It is interesting to note that the strength of **L5rHBc** forming a hydrogen bond with Trp35 in the ferrous state (k^a = 0.005 mDyn/Å), is much smaller than the strength of this hydrogen bond in the ferric state (k^a = 0.106 mDyn/Å), which is consistent with **L4** in the ferric state, where the ligand does not form a hydrogen bonds with Trp35.

The last ligand investigated in this study **L6** has a hydroxy group in the *meta* position of the phenyl ring, and forms three hydrogen bonds in the ferric state (white blue marks in Figure 7a), namely such as **L6oHBa** (circle), **L6oHBb** (triangle), and **L6oHBc** (square). The characters of these hydrogen bonds are the same as in **L5**, and have similar strengths (k^a = 0.685, 0.159, and 0.061 mDyn/Å, respectively). In the ferrous state (white blue marks in Figure 7b) **L6** forms three hydrogen bonds (**L6rHBa**, **L6rHBb**, and **L6rHBc**) with the same character, and slightly smaller strengths (k^a = 0.524, 0.188, and 0.011 mDyn/Å, respectively).

Generally, according to Figure 7a, the average strength the hydrogen bonds in the ferric state of the protein, is bigger than the strength of the hydrogen bond in the water dimer (k^a = 0.282

and 0.214 mDyn/Å, respectively). The strongest hydrogen bonds in this oxidation state (circles in Figures 3, 4, 7a, and S2–S5), are of the N–H ⋯ O character, where the hydrogen atom donor is from the ligand, and the oxygen atom is from Pro69. The weakest hydrogen bonds in this oxidation state (squares in Figures 3, 4, 7a, and S2–S5) are generally of the O–H ⋯ O character, where the hydrogen atom donor is from the ligand, and the oxygen atom is from Glu81, or of the N–H ⋯ O character, where the hydrogen atom donor is from Trp35, and the oxygen atom is from the ligand. Similarly according to Figure 7b, the average strength of the hydrogen bonds in the ferrous state, is bigger than in the water dimer ($k^a = 0.264$ and 0.214 mDyn/Å, respectively), and the strongest hydrogen bonds are of the N–H ⋯ O character where the ligand acts as a hydrogen atom donor, while the weakest are of the O–H ⋯ O character where the ligands acts as a hydrogen atom donor, and of the N–H ⋯ O character, where the protein acts as a hydrogen atom donor.

Figure 7c,d present relations between the local mode force constant, and the hydrogen bond length, disclosing a relatively good correlation between those two properties in the ferric state ($R^2 = 0.9758$), and in the ferrous state ($R^2 = 0.9830$). Generally, according to our results a stronger hydrogen bond relatively good correlates with a shorter bond length, which is consistent with the general power relation between these two bond properties [98].

4 | Conclusions

In this study, we computationally investigated the strength of the FeS chemical bonds in the heme groups and the hydrogen bonds between molecular inhibitors and the binding sites of bacterioferritin from *Pseudomonas aeruginosa*. The calculations were based on available experimental structures of six ligands in the protein and involved QM/MM geometry optimizations and vibrational frequency analyses. Each QM/MM system included two protein chains connected by a heme group through the side chains of two methionine residues, with the heme, side chains, and ligand treated at the QM level and the remainder of the protein at the MM level, in both the ferric and ferrous oxidation states.

Our results show that in the ferric state the FeS chemical bonds are stronger, shorter, more covalent, and less polar than in the gas phase, with two notable outliers: the protein with ligand **L6** and the gas-phase model. In the ferrous state, the FeS bonds are also stronger, shorter, and more covalent than in the gas phase, though their polarity is comparable. Overall, the transition from ferric to ferrous weakens the FeS bond, making it shorter, less covalent, and less polar, a trend that is consistent with our gas-phase calculations. For the hydrogen bonds, the average bond strength in both oxidation states exceeded that of a water dimer, highlighting the stabilizing effect of the protein environment. The strongest hydrogen bonds were typically of the N–H ⋯ O type, with the hydrogen donor originating from the ligand and the acceptor oxygen from Pro69. The weakest interactions were generally O–H ⋯ O bonds, with the donor from the ligand and the acceptor oxygen from Glu81, or N–H ⋯ O bonds, where the donor was Trp35 and the acceptor oxygen from the ligand.

Taken together, these results provide molecular-level insights into the interplay between oxidation state, bond strength, and the surrounding protein environment (or matrix). They demonstrate how the protein environment modulates both covalent and noncovalent interactions, providing insights into the mechanisms that influence electron transfer and Fe binding and release in bacterioferritin. Beyond these mechanistic findings, the results may inform the design of antibacterial strategies targeting ferritin-related pathways and support the development of ferritin-based nano-materials for biomedical applications.

Acknowledgments

This work was financially supported by the National Science Foundation, grant number CHE 2102461. Computational resources provided by SMU's O'Donnell Institute of Data Science and High Performance Computing.

Conflicts of Interest

The authors declare no conflicts of interest.

Data Availability Statement

The data that support the findings of this study are available from the corresponding author upon reasonable request.

References

1. M. U. Muckenthaler, S. Rivella, M. W. Hentze, and B. Galy, "A Red Carpet for Iron Metabolism," *Cell* 168, no. 3 (2017): 344–361.

2. K. Eshelman, H. Yao, A. N. D. Punchi Hewage, J. J. Deay, J. R. Chandler, and M. Rivera, "Inhibiting the Bfrb:Bfd Interaction in *Pseudomonas Aeruginosa* Causes Irreversible Iron Accumulation in Bacterioferritin and Iron Deficiency in the Bacterial Cytosol," *Metallomics* 9, no. 6 (2017): 646–659.

3. M. Rivera, "Bacterioferritin: Structure, Dynamics, and Protein–Protein Interactions at Play in Iron Storage and Mobilization," *Accounts of Chemical Research* 50, no. 2 (2017): 331–340.

4. A. N. D. Punchi Hewage, H. Yao, B. Nammalwar, et al., "Small Molecule Inhibitors of the Bfrb–Bfd Interaction Decrease *Pseudomonas Aeruginosa* Fitness and Potentiate Fluoroquinolone Activity," *Journal of the American Chemical Society* 141, no. 20 (2019): 8171–8184.

5. S. C. Andrews, "The Ferritin-like Superfamily: Evolution of the Biological Iron Storeman from a Rubrerythrin-like Ancestor," *Biochimica et Biophysica Acta* 1800, no. 8 (2010): 691–705.

6. L. Swartz, M. Kuchinskas, H. Li, T. L. Poulos, and W. N. Lanzilotta, "Redox–Dependent Structural Changes in the *Azotobacter Vinelandii Bacterioferritin*: New Insights into the Ferroxidase and Iron Transport Mechanism," *Biochemistry* 45, no. 14 (2006): 4421–4428.

7. C. Jobichen, T. Ying Chong, R. Rattinam, et al., "Bacterioferritin Nanocage Structures Uncover the Biomineralization Process in Ferritins," *PNAS Nexus* 2, no. 7 (2023): e235.1–e235.9.

8. G. Khare, P. Nangpal, and A. K. Tyagi, "Differential Roles of Iron Storage Proteins in Maintaining the Iron Homeostasis in *Mycobacterium Tuberculosis*," *PLoS One* 12, no. 1 (2017): e0169545.1–e0169545.18.

9. A. Mohanty, A. Parida, B. Subhadarshanee, et al., "Alteration of Coaxial Heme Ligands Reveals the Role of Heme in Bacterioferritin from *Mycobacterium Tuberculosis*," *Inorganic Chemistry* 60, no. 22 (2021): 16,937–16,952.

10. J. Pullin, J. M. Bradley, G. R. Moore, N. E. Le Brun, M. T. Wilson, and D. A. Svistunenko, "Electron Transfer from Haem to the Di–Iron

Ferroxidase Centre in Bacterioferritin," *Angewandte Chemie, International Edition* 60, no. 15 (2021): 8376–8379.

11. M. A. Quail, P. Jordan, J. M. Grogan, et al., "Spectroscopic and Voltammetric Characterisation of the Bacterioferritin-Associated Ferredoxin Ofescherichia Coli," *Biochemical and Biophysical Research Communications* 229, no. 2 (1996): 635–642.

12. M. Rivera, "Mobilization of Iron Stored in Bacterioferritin, a New Target for Perturbing Iron Homeostasis and Developing Antibacterial and Antibiofilm Molecules," *Journal of Inorganic Biochemistry* 247 (2023): 112306.1–112306.17.

13. A. Soldano, H. Yao, A. N. D. Punchi Hewage, et al., "Small Molecule Inhibitors of the Bacterioferritin (Bfrb)–Ferredoxin (Bfd) Complex Kill Biofilm-Embedded *Pseudomonas Aeruginosa* Cells," *ACS Infectious Diseases* 7, no. 1 (2021): 123–140.

14. A. M. van der Ven, H. Gyamfi, U. Suttisansanee, et al., "Molecular Engineering of E. Coli Bacterioferritin: a Versatile Nanodimensional Protein Cage," *Molecules* 28, no. 12 (2023): 4663.1–4663.29.

15. Y. Wang, H. Yao, Y. Cheng, et al., "Characterization of the Bacterioferritin/Bacterioferritin Associated Ferredoxin Protein–Protein Interaction in Solution and Determination of Binding Energy Hot Spots," *Biochemistry* 54, no. 40 (2015): 6162–6175.

16. S. K. Weeratunga, C. E. Gee, S. Lovell, Y. Zeng, C. L. Woodin, and M. Rivera, "Binding of *Pseudomonas Aeruginosa* Apobacterioferritin–Associated Ferredoxin to Bacterioferritin B Promotes Heme Mediation of Electron Delivery and Mobilization of Core Mineral Iron," *Biochemistry* 48, no. 31 (2009): 7420–7431.

17. S. K. Weeratunga, S. Lovell, H. Yao, et al., "Structural Studies of Bacterioferritin B from *Pseudomonas Aeruginosa* Suggest a Gating Mechanism for Iron Uptake via the Ferroxidase Center," *Biochemistry* 49, no. 6 (2010): 1160–1175.

18. S. Wong, R. Abdulqadir, N. Le Brun, G. Moore, and A. Mauk, "Fe–Haem Bound to *Escherichia Coli* Bacterioferritin Accelerates Iron Core Formation by an Electron Transfer Mechanism," *Biochemical Journal* 444, no. 3 (2012): 553–560.

19. H. Yao, A. Soldano, L. Fontenot, et al., "*Pseudomonas Aeruginosa* Bacterioferritin is Assembled from Ftna and Bfrb Subunits with the Relative Proportions Dependent on the Environmental Oxygen Availability," *Biomolecules* 12, no. 3 (2022): 366.1–366.19.

20. H. Yao, Y. Wang, S. Lovell, et al., "the Structure of the Bfrb–Bfd Complex Reveals Protein–Protein Interactions Enabling Iron Release from Bacterioferritin," *Journal of the American Chemical Society* 134, no. 32 (2012): 13,470–13,481.

21. S. Yasmin, S. C. Andrews, G. R. Moore, and N. E. Le Brun, "A New Role for Heme, Facilitating Release of Iron from the Bacterioferritin Iron Biomineral," *Journal of Biological Chemistry* 286, no. 5 (2011): 3473–3483.

22. V. Guallar and F. H. Wallrapp, "QM/MM Methods: Looking inside Heme Proteins Biochemisty," *Biophysical Chemistry* 149, no. 1 (2010): 1–11.

23. M. W. van der Kamp and M. J. Mulholland, "Combined Quantum Mechanics/Molecular Mechanics (QM/MM) Methods in Computational Enzymology," *Biochemistry* 52, no. 16 (2013): 2708–2728.

24. D. A. Case, I. Y. Ben-Shalom, S. R. Brozell, et al., *AMBER* (University of California, 2018).

25. W. L. Jorgensen, J. Chandrasekhar, J. D. Madura, R. W. Impey, and M. L. Klein, "Comparison of Simple Potential Functions for Simulating Liquid Water," *Journal of Chemical Physics* 79, no. 2 (1983): 926–935.

26. L. W. Chung, W. M. C. Sameera, R. Ramozzi, et al., "The ONIOM Method and Its Applications," *Chemical Reviews* 115 (2015): 5678–5796.

27. C. Adamo and V. Barone, "Toward Reliable Density Functional Methods without Adjustable Parameters: The PBE0 Model," *Journal of Chemical Physics* 110, no. 13 (1999): 6158–6170.

28. R. Ditchfield, W. J. Hehre, and J. A. Pople, "Self–Consistent Molecular–Orbital Methods. IX. an Extended Gaussian–Type Basis for Molecular–Orbital Studies of Organic Molecules," *Journal of Chemical Physics* 54 (1971): 724–728.

29. C. J. Cramer and D. G. Truhlar, "Density Functional Theory for Transition Metals and Transition Metal Chemistry," *Physical Chemistry Chemical Physics* 11, no. 46 (2009): 10,757–10,816.

30. S. Li, J. M. Hennigan, D. A. Dixon, and K. A. Peterson, "Accurate Thermochemistry for Transition Metal Oxide Clusters," *Journal of Physical Chemistry. A* 113, no. 27 (2009): 7861–7877.

31. S. Zhao, Z.-H. Li, W.-N. Wang, et al., "Is the Uniform Electron Gas Limit Important for Small Ag Clusters? Assessment of Different Density Functionals for Ag_n ($n<4$)," *Journal of Chemical Physics* 124, no. 18 (2006): 184102.

32. M. Freindorf, A. A. A. Delgado, and E. Kraka, "CO Bonding in Hexa– and Pentacoordinate Carboxy–Neuroglobin—A QM/MM and Local Vibrational Mode Study," *Journal of Computational Chemistry* 43 (2022): 1725–1746.

33. M. Freindorf and E. Kraka, "Critical Assessment of the FeC and CO Bond strength in Carboxymyoglobin—A QM/MM Local Vibrational Mode Study," *Journal of Molecular Modeling* 26 (2020): 281–1–281–15.

34. M. K. Safo, G. P. Gupta, F. A. Walker, and W. R. Scheidt, "Models of the Cytochromes B. Control of Axial Ligand Orientation with a Hindered Porphyrin System," *Journal of the American Chemical Society* 113, no. 15 (1991): 5497–5510.

35. E. Kraka, W. Zou, and Y. Tao, "Decoding Chemical Information from Vibrational Spectroscopy Data: Local Vibrational Mode Theory," *WIREs Computational Molecular Science* 10 (2020): 1480.

36. D. Cremer, J. A. Larsson, and E. Kraka, "New Developments in the Analysis of Vibrational Spectra on the Use of Adiabatic Internal Vibrational Modes," in *Theoretical and Computational Chemistry*, ed. C. Parkanyi (Elsevier, 1998), 259–327.

37. Z. Konkoli and D. Cremer, "A New Way of Analyzing Vibrational Spectra. I. Derivation of Adiabatic Internal Modes," *International Journal of Quantum Chemistry* 67 (1998): 1–9.

38. Z. Konkoli and D. Cremer, "A New Way of Analyzing Vibrational Spectra. III. Characterization of Normal Vibrational Modes in terms of Internal Vibrational Modes," *International Journal of Quantum Chemistry* 67 (1998): 29–40.

39. Z. Konkoli, J. A. Larsson, and D. Cremer, "A New Way of Analyzing Vibrational Spectra. II. Comparison of Internal Mode Frequencies," *International Journal of Quantum Chemistry* 67 (1998): 11–27.

40. Z. Konkoli, J. A. Larsson, and D. Cremer, "A New Way of Analyzing Vibrational Spectra. IV. Application and Testing of Adiabatic Modes within the Concept of the Characterization of Normal Modes," *International Journal of Quantum Chemistry* 67 (1998): 41–55.

41. D. Cremer and E. Kraka, "From Molecular Vibrations to Bonding, Chemical Reactions, and Reaction Mechanism," *Current Organic Chemistry* 14 (2010): 1524–1560.

42. D. Cremer, A. Wu, J. A. Larsson, and E. Kraka, "Some Thoughts about Bond Energies, Bond Lengths, and Force Constants," *Journal of Molecular Modeling* 6 (2000): 396–412.

43. A. A. A. Delgado, A. Humason, R. Kalescky, M. Freindorf, and E. Kraka, "Exceptionally Long Covalent CC Bonds—A Local Vibrational Mode Study," *Molecules* 26 (2021): 950–1–950–25.

44. A. Humason, W. Zou, and D. Cremer, "11,11-Dimethyl-1,6-methano[10]annulene-An Annulene with an Ultralong CC Bond or a Fluxional Molecule?," *Journal of Physical Chemistry. A* 119 (2014): 1666–1682.

45. R. Kalescky, E. Kraka, and D. Cremer, "Identification of the Strongest Bonds in Chemistry," *Journal of Physical Chemistry. A* 117 (2013): 8981–8995.

46. R. Kalescky, E. Kraka, and D. Cremer, "Are Carbon-Halogen Double and Triple Bonds Possible?," *International Journal of Quantum Chemistry* 114 (2014): 1060–1072.

47. R. Kalescky, W. Zou, E. Kraka, and D. Cremer, "Quantitative Assessment of the Multiplicity of Carbon-Halogen Bonds: Carbenium and Halonium Ions with F, Cl, Br, and I," *Journal of Physical Chemistry. A* 118 (2014): 1948–1963.

48. E. Kraka and D. Cremer, "Weaker Bonds with Shorter Bond Lengths," *Revista Processos Químicos* 6 (2012): 39–42.

49. E. Kraka, J. A. Larsson, and D. Cremer, "Generalization of the Badger Rule Based on the Use of Adiabatic Vibrational Modes," in *Computational Spectroscopy*, ed. J. Grunenberg (Wiley, 2010), 105–149.

50. E. Kraka, D. Setiawan, and D. Cremer, "Re-Evaluation of the Bond Length-Bond Strength Rule: The Stronger Bond Is not Always the Shorter Bond," *Journal of Computational Chemistry* 37 (2015): 130–142.

51. J. A. Larsson and D. Cremer, "Theoretical Verification and Extension of the Mckean Relationship between Bond Lengths and Stretching Frequencies," *Journal of Molecular Structure* 485 (1999): 385–407.

52. D. Setiawan, E. Kraka, and D. Cremer, "Hidden Bond Anomalies: The Peculiar Case of the Fluorinated Amine Chalcogenides," *Journal of Physical Chemistry. A* 119 (2015): 9541–9556.

53. D. Setiawan, D. Sethio, D. Cremer, and E. Kraka, "From Strong to Weak NF Bonds: On the Design of a New Class of Fluorinating Agents," *Physical Chemistry Chemical Physics* 20 (2018): 23,913–23,927.

54. W. Zou and D. Cremer, "C_2 in a Box: Determining its Intrinsic Bond Strength for the $X^1\Sigma^+_g$ Ground State," *Chemistry - A European Journal* 22 (2016): 4087–4099.

55. V. Oliveira and D. Cremer, "Transition from Metal–Ligand Bonding to Halogen Bonding Involving a Metal as Halogen Acceptor: A Study of Cu, Ag, Au, Pt, and Hg Complexes," *Chemical Physics Letters* 681 (2017): 56–63.

56. V. Oliveira, D. Cremer, and E. Kraka, "The Many Facets of Chalcogen Bonding: Described by Vibrational Spectroscopy," *Journal of Physical Chemistry. A* 121 (2017): 6845–6862.

57. V. Oliveira and E. Kraka, "Systematic Coupled Cluster Study of Noncovalent Interactions Involving Halogens, Chalcogens, and Pnicogens," *Journal of Physical Chemistry. A* 121 (2017): 9544–9556.

58. V. Oliveira, E. Kraka, and D. Cremer, "Quantitative Assessment of Halogen Bonding Utilizing Vibrational Spectroscopy," *Inorganic Chemistry* 56 (2016): 488–502.

59. V. Oliveira, E. Kraka, and D. Cremer, "The Intrinsic Strength of the Halogen Bond: Electrostatic and Covalent Contributions Described by Coupled Cluster Theory," *Physical Chemistry Chemical Physics* 18 (2016): 33,031–33,046.

60. V. P. Oliveira, E. Kraka, and F. B. C. Machado, "Pushing 3c-4e bonds to the limit: A coupled cluster study of stepwise fluorination of first-row atoms," *Inorganic Chemistry* 58 (2019): 14,777–14,789.

61. V. P. Oliveira, B. L. Marcial, F. B. C. Machado, and E. Kraka, "Metal-Halogen Bonding Seen through the Eyes of Vibrational Spectroscopy," *Materials* 13 (2020): 55.

62. D. Sethio, V. Oliveira, and E. Kraka, "Quantitative Assessment of Tetrel Bonding Utilizing Vibrational Spectroscopy," *Molecules* 23 (2018): 2763–1–2763–21.

63. D. Setiawan and D. Cremer, "Super-Pnicogen Bonding in the Radical Anion of the Fluorophosphine Dimer," *Chemical Physics Letters* 662 (2016): 182–187.

64. D. Setiawan, E. Kraka, and D. Cremer, "Description of Pnicogen Bonding with the help of Vibrational Spectroscopy-The Missing Link Between Theory and Experiment," *Chemical Physics Letters* 614 (2014): 136–142.

65. D. Setiawan, E. Kraka, and D. Cremer, "Strength of the Pnicogen Bond in Complexes Involving Group VA Elements N, P, and As," *Journal of Physical Chemistry. A* 119 (2014): 1642–1656.

66. Y. Tao, Y. Qiu, W. Zou, S. Nanayakkara, S. Yannacone, and E. Kraka, "In Situ Assessment of Intrinsic Strength of X-I ... OA Type Halogen Bonds in Molecular Crystals with Periodic Local Vibrational Mode Theory," *Molecules* 25 (2020): 1589.

67. S. Yannacone, V. Oliveira, N. Verma, and E. Kraka, "A Continuum from Halogen Bonds to Covalent Bonds: Where Do λ^3 Iodanes Fit?," *Inorganics* 7 (2019): 47.

68. X. Zhang, H. Dai, H. Yan, W. Zou, and D. Cremer, "B-H π Interaction: A New Type of Nonclassical Hydrogen Bonding," *Journal of the American Chemical Society* 138 (2016): 4334–4337.

69. W. Zou, X. Zhang, H. Dai, H. Yan, D. Cremer, and E. Kraka, "Description of an Unusual Hydrogen Bond Between Carborane and a Phenyl Group," *Journal of Organometallic Chemistry* 856 (2018): 114–127.

70. N. Beiranvand, M. Freindorf, and E. Kraka, "Hydrogen Bonding in Natural and Unnatural Base Pairs—Explored with Vibrational Spectroscopy," *Molecules* 26 (2021): 2268–1–2268–22.

71. M. Freindorf, E. Kraka, and D. Cremer, "A Comprehensive Analysis of Hydrogen Bond Interactions Based on Local Vibrational Modes," *International Journal of Quantum Chemistry* 112 (2012): 3174–3187.

72. M. Freindorf, Y. Tao, D. Sethio, D. Cremer, and E. Kraka, "New Mechanistic Insights into the Claisen Rearrangement of Chorismate—A Unified Reaction Valley Approach Study," *Molecular Physics* 117 (2018): 1172–1192.

73. R. Kalescky, E. Kraka, and D. Cremer, "Local Vibrational Modes of the Formic Acid Dimer—The Strength of the Double H-Bond," *Molecular Physics* 111 (2013): 1497–1510.

74. R. Kalescky, W. Zou, E. Kraka, and D. Cremer, "Local Vibrational Modes of the Water Dimer—Comparison of Theory and Experiment," *Chemical Physics Letters* 554 (2012): 243–247.

75. R. Kalescky, W. Zou, E. Kraka, and D. Cremer, "Vibrational Properties of the Isotopomers of the Water Dimer Derived from Experiment and Computations," *Australian Journal of Chemistry* 67 (2014): 426.

76. S. Lyu, N. Beiranvand, M. Freindorf, and E. Kraka, "Interplay of Ring Puckering and Hydrogen Bonding in Deoxyribonucleosides," *Journal of Physical Chemistry. A* 123 (2019): 7087–7103.

77. M. Z. Makoś, M. Freindorf, D. Sethio, and E. Kraka, "New Insights into Fe–H_2 and Fe–H^- Bonding of a [NiFe] Hydrogenase Mimic—A Local Vibrational Mode Study," *Theoretical Chemistry Accounts* 138 (2019): 76.

78. Y. Tao, W. Zou, J. Jia, W. Li, and D. Cremer, "Different Ways of Hydrogen Bonding in Water—Why Does Warm Water Freeze Faster than Cold Water?," *Journal of Chemical Theory and Computation* 13 (2017): 55–76.

79. Y. Tao, W. Zou, and E. Kraka, "Strengthening of Hydrogen Bonding With the Push-Pull Effect," *Chemical Physics Letters* 685 (2017): 251–258.

80. S. Yannacone, D. Sethio, and E. Kraka, "Quantitative Assessment of Intramolecular Hydrogen Bonds in Neutral Histidine," *Theoretical Chemistry Accounts* 139 (2020): 125–1–125–10.

81. I. Mayer, "Charge, Bond Brder an Valence in the Ab Initio Theory," *Chemical Physics Letters* 97 (1983): 270–274.

82. I. Mayer, "Bond Orders and Valences from Ab Initio Wave Functions," *International Journal of Quantum Chemistry* 29 (1986): 477–483.

83. I. Mayer, "Bond Order and Valence Indices: a Personal Account," *Journal of Computational Chemistry* 28, no. 1 (2007): 204–221.

84. R. F. W. Bader, "A Quantum Theory of Molecular Structure and Its Applications," *Chemical Reviews* 91, no. 5 (1991): 893–928.

85. R. F. W. Bader, *Atoms in Molecules: A Quantum Theory (International Series of Monographs on Chemistry)* (Clarendon Press, 1994).

86. R. F. W. Bader, "the Quantum Mechanical Basis of Conceptual Chemistry," *Monatshefte for Chemie* 136, no. 6 (2005): 819–854.

87. D. Cremer and E. Kraka, "Chemical Bonds without Bonding Electron Density? Does the Difference Electron-Density Analysis Suffice for a Description of the Chemical Bond?," *Angewandte Chemie, International Edition* 23 (1984): 627–628.

88. D. Cremer and E. Kraka, "A Description of the Chemical Bond in Terms of Local Properties of Electron Density and Energy," *Croatica Chemica Acta* 57 (1984): 1259–1281.

89. E. Kraka and D. Cremer, "Chemical Implication of Local Features of the Electron Density Distribution," in *Theoretical Models of Chemical Bonding. The Concept of the Chemical Bond, Volume 2*, ed. Z. B. Maksic (Springer Verlag, 1990), 453–542.

90. M. J. Frisch, G. W. Trucks, H. B. Schlegel, et al., *Gaussian 16* (Gaussian Inc., 2016).

91. W. Zou, R. Moura, Jr., C. V. Santos-Jr, et al., *LModeA2025. Computational and Theoretical Chemistry Group (CATCO)* (Southern Methodist University, 2025).

92. A. E. Reed, L. A. Curtiss, and F. Weinhold, "Intermolecular Interactions from a Natural Bond Orbital, Donor-Acceptor Viewpoint," *Chemical Reviews* 88 (1988): 899–926.

93. T. A. Keith, *AIMALL* (TK Gristmill Software, 2017).

94. M. Kaupp, B. Metz, and H. Stoll, "Breakdown of Bond Length–Bond Strength Correlation: a Case Study," *Angewandte Chemie, International Edition* 39, no. 24 (2000): 4607–4609.

95. M. Kaupp and S. Riedel, "on the Lack of Correlation between Bond Lengths, Dissociation Energies, and Force Constants: the Fluorine–Substituted Ethane Homologues," *Inorganica Chimica Acta* 357, no. 6 (2004): 1865–1872.

96. B. A. Lindquist and T. H. Dunning, "Bonding in $FSSF_3$: Breakdown in Bond Length–Strength Correlations and Implications for SF_2 Dimerization," *Journal of Physical Chemistry Letters* 4, no. 18 (2013): 3139–3143.

97. M. Freindorf, Y. Shao, T. R. Furlani, and J. Kong, "Lennard-Jones Parameters for the Combined QM/MM Method Using the B3LYP/6-31G*/AMBER Potential," *Journal of Computational Chemistry* 26, no. 12 (2005): 1270–1278.

98. G. V. Gibbs, F. C. Hill, M. B. Boisen, and R. T. Downs, "Power Law Relationships between Bond Length, Bond Strength and Electron Density Distributions," *Physics and Chemistry of Minerals* 25, no. 8 (1998): 585–590.

Supporting Information

Additional supporting information can be found online in the Supporting Information section. **Data S1:** Supporting Information.